

Design of Wide-Bandwidth Envelope-Tracking Power Amplifiers for OFDM Applications

Feipeng Wang, *Student Member, IEEE*, Annie Hueiching Yang, *Student Member, IEEE*, Donald F. Kimball, *Member, IEEE*, Lawrence E. Larson, *Fellow, IEEE*, and Peter M. Asbeck, *Fellow, IEEE*

Abstract—An efficiency-enhanced power-amplifier system design is presented based on wide-bandwidth envelope tracking (WBET) with application to orthogonal frequency-division multiplexing wireless local area network systems. Envelope elimination and restoration (EER) and WBET are compared in terms of the time mismatch sensitivity between the base-band amplitude path and the RF path, and it is demonstrated that WBET is much less sensitive than EER to these effects. An adaptive time-alignment algorithm for the WBET system is developed and demonstrated. The analysis and algorithm are verified by experimental results. The measurement shows that the peak drain efficiency of the complete system was 30% at a 2.4-GHz orthogonal frequency-division multiplexing output power of 20 dBm.

Index Terms—Envelope elimination and restoration (EER), envelope tracking (ET), orthogonal frequency-division multiplexing (OFDM), power amplifiers, power tracking, time alignment, wireless local area network (WLAN).

I. INTRODUCTION

HIGH-EFFICIENCY RF power amplifiers (PAs) are critical in portable battery-operated wireless communication systems (such as cellular phones, personal digital assistants, and laptops) because they can dominate the power consumption [1], [2]. PAs demonstrate the highest efficiency when operated in the compression region (such as in Class-A, Class-AB and Class-B modes) or in the switching mode (such as Class D, E, F) [3]–[5]. However, these highly efficient nonlinear PAs can only amplify constant envelope modulation signals [such as global system for mobile communications (GSM)] without nonlinear distortion. With modern wireless communication systems evolving to more spectrally efficient and higher data-rate modulation formats, highly linear PAs are required to avoid the out-of-channel interference [e.g., adjacent channel power ratio (ACPR)] and distortion [e.g., error vector magnitude (EVM)].

Manuscript received May 24, 2004; revised September 28, 2004. This work was supported by the Powerwave Corporation, the Ericsson Corporation, and the Conexant Corporation under the University of California Microelectronics Innovation and Computer Research Opportunities and University of California Discovery Grant Programs.

F. Wang, D. F. Kimball, L. E. Larson, and P. M. Asbeck are with the Center for Wireless Communications, Department of Electrical and Computer Engineering, University of California at San Diego, La Jolla, CA 92092 USA (e-mail: wangfp@cw.cucsd.edu; dkimball@cw.cucsd.edu; larson@ece.ucsd.edu; asbeck@ece.ucsd.edu).

A. H. Yang was with the Center for Wireless Communications, Department of Electrical and Computer Engineering, University of California at San Diego, La Jolla, CA 92092 USA. She is now with the Space and Naval Warfare System Center, San Diego, CA 92152 USA (e-mail: anniey@spawar.navy.mil).

Digital Object Identifier 10.1109/TMTT.2005.845716

TABLE I
802.11 G WLAN TRANSMITTER SPECIFICATIONS

Frequency band	2.4-2.4835GHz
Numbers of Carriers	52 (48 data and 4 pilots)
Channel bandwidth	16.25MHz
Data rate	6 to 54Mbps
Carrier type	OFDM
Modulation	BPSK, QPSK, 16QAM or 64QAM
Max. instantaneous output power	1W (in USA)
EVM	5.6% or -25dB for 54Mbps
Spectrum mask	-20dBc @ 11MHz offset -28dBc @ 20MHz offset -40dBc @ 30MHz offset

For example, the wireless local area network (WLAN) 802.11 g standard employs 64-QAM modulation and 52 orthogonal frequency division multiplexing (OFDM) carriers at a 54-Mb/s data rate. This modulation format has a high envelope peak-average ratio (PAR) of 8–10 dB. The WLAN 802.11 g specifications for the transmitter design are summarized in Table I [6], [7].

The traditional approach to linearly amplify the nonconstant envelope modulated signal is to “back off” the linear Class-A or Class-AB PA’s output power until the distortion level is within acceptable limits. Unfortunately, this lowers efficiency significantly, especially for high PAR signals. Thus, there is an inherent tradeoff between linearity and efficiency in PA design.

This problem has been thoroughly investigated over many years and envelope elimination and restoration (EER) [8]–[10], predistortion [3], [4], feedback [3], [4], feed-forward [4], Doherty [11], envelope tracking (ET) [12]–[15], linear amplification with nonlinear control (LINC) [16], and gate dynamic biasing [17], [18] are just some of the techniques explored.

Power supply control schemes offer the greatest potential for high-efficiency operation for high PAR signals. There are three traditional dynamic power-supply control schemes for PA efficiency enhancement: EER [8]–[10], wide-bandwidth envelope tracking (WBET) [12], and average envelope tracking (AET) [13], [14]. Figs. 1 and 2 show the block diagrams of the traditional EER and envelope-tracking (ET) systems. EER uses a combination of a switching-mode PA and an envelope remodulation circuit. ET utilizes a linear PA and a supply modulation circuit where the supply voltage tracks the input envelope. The WBET scheme tracks the instantaneous wide-bandwidth input envelope signal power, whereas the AET scheme follows the long-term average input envelope signal power. This later

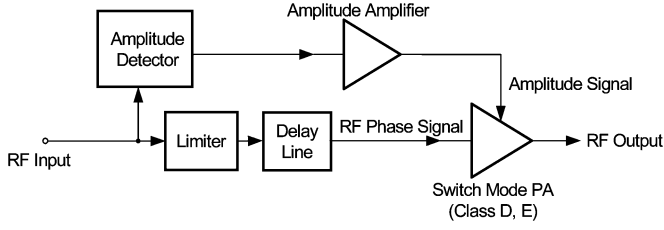


Fig. 1. Block diagram of EER system.

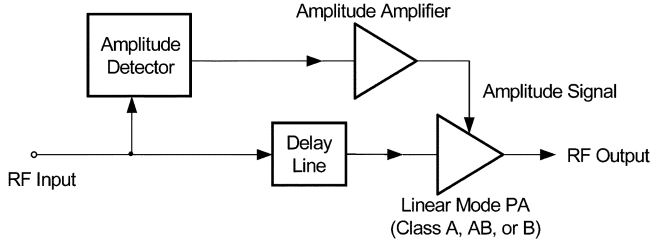


Fig. 2. Block diagram of ET system. The bandwidth of the amplitude detector determines whether the system responds to the long-term average of the envelope—AET—or the instantaneous variations in the envelope—WBET.

approach is especially useful for systems with dynamic power control—such as the reverse link in code division multiple access (CDMA) [19]. Section II will discuss the WBET system design, which exhibits nearly the same potential efficiency improvements as EER, but is less sensitive to path mismatch effects.

Even though both EER and WBET are promising for WLAN OFDM signals, two important issues for both schemes are the time alignment between the base-band amplitude path and the RF path and the wide-band high-efficiency envelope amplifier design. In this paper, we focus on the time alignment between the envelope and RF paths in order to minimize the distortion and EVM. Section II compares the sensitivity of the EER and WBET schemes to time misalignment, and Section III presents a technique for optimizing the alignment between the baseband amplitude and RF paths.

Section IV presents the experimental performance of the WBET system with digital predistortion for a WLAN 802.11 OFDM application.

II. WBET SYSTEM DESIGN

The block diagram of the proposed ET system is shown in Fig. 3. The amplitude signal is calculated from the complex baseband signal and amplified by the amplitude amplifier, providing a dynamic drain voltage to the RF transistor. The amplitude is $A = (I^2 + Q^2)^{1/2}$, where I and Q are the real and imaginary parts of the complex baseband signal. At the same time, the digital IF signal is upconverted and amplified by the RF power transistor biased (in our case) in the Class-AB region.

The two important system related issues for the WBET amplifier design are the optimum biasing of the amplifier to achieve maximum power-added efficiency (PAE) and the time alignment of the RF and baseband amplitude signals.

A. Optimum Efficiency Biasing of the ET Amplifier

As a first step, the power amplifier can be modeled as having three independent inputs (P_{RFIn} , V_{DD} , and V_{GG}) and two outputs (P_{RFout} and I_{DD}) i.e.,

$$P_{\text{RFout}} = f_1(P_{\text{RFIn}}, V_{\text{DD}}, V_{\text{GG}}) \quad (1a)$$

$$I_{\text{DD}} = f_2(P_{\text{RFIn}}, V_{\text{DD}}, V_{\text{GG}}) \quad (1b)$$

where P_{RFIn} and P_{RFout} refer to the input and output RF signal powers, V_{DD} is the dynamic drain supply voltage, V_{GG} is the dynamic gate biasing voltage, and I_{DD} is the dynamic drain supply current.

Since the output power probability density function is fixed [6], [7], we can control the independent variables P_{RFIn} , V_{DD} , and V_{GG} to obtain the highest PAE at each output power. For example, Fig. 4 shows a single-tone ADS simulation of the optimal (in the sense of highest PAE) P_{RFIn} , V_{DD} , and V_{GG} for the 2.4-GHz GaAs MESFET Class-AB power amplifier described in Section IV.

Based on the probability density function of the RF signal, the average drain efficiency can be calculated as [12], [19]

$$\eta_{\text{ave}} = \frac{\int_0^{P_{\text{RFout,max}}} p(P_{\text{RFout}}) P_{\text{RFout}} dP_{\text{RFout}}}{\int_0^{P_{\text{RFout,max}}} p(P_{\text{RFout}}) V_{\text{DD}}(P_{\text{RFout}}) I_{\text{DD}}(P_{\text{RFout}}) dP_{\text{RFout}}} \quad (2)$$

where $V_{\text{DD}}(P_{\text{RFout}})$ and $I_{\text{DD}}(P_{\text{RFout}})$ are the drain voltage and drain current, which are the functions of the output RF signal power P_{RFout} , and $p(P_{\text{RFout}})$ is the probability function of the output power.

Note from Fig. 4 that the optimal V_{DD} curves coincide with the theoretical envelope given by $V_{\text{DD,opt}} = (R_L P_{\text{out}})^{1/2}$, where R_L is the load resistor of the transistor, so a linear transformation of the baseband amplitude signal is optimum for the envelope amplifier. Also note that a constant V_{GG} provides nearly optimal performance, where the device is biased deeply into the Class-AB mode.

The wide gain variation illustrated in Fig. 4 will result in significant nonlinear distortion and poor EVM. We describe an improved baseband AM-AM and AM-PM predistortion technique in Section IV to improve the linearity so that the ACPR and EVM requirements are met. Fig. 5 shows a comparison of simulated PAE between the constant V_{DD} Class-AB performance and “ideal” ET performance using the biasing approach of Fig. 4. Note that the PAE is improved significantly over a wide range of output powers.

Another important issue is determination of the optimum *minimum* drain voltage when P_{RFIn} approaches zero. Table II compares the simulated EVM and efficiency results between the fixed-bias Class-AB PA ($V_{\text{DD}} = 4.4$ V) and two ET amplifiers with $V_{\text{DD,min}} = 0$ and 0.5 V, respectively. The ET $V_{\text{DD,min}} = 0.5$ V case provides both improved linearity and PAE, due to the higher gain at $V_{\text{DD}} = 0.5$ V.

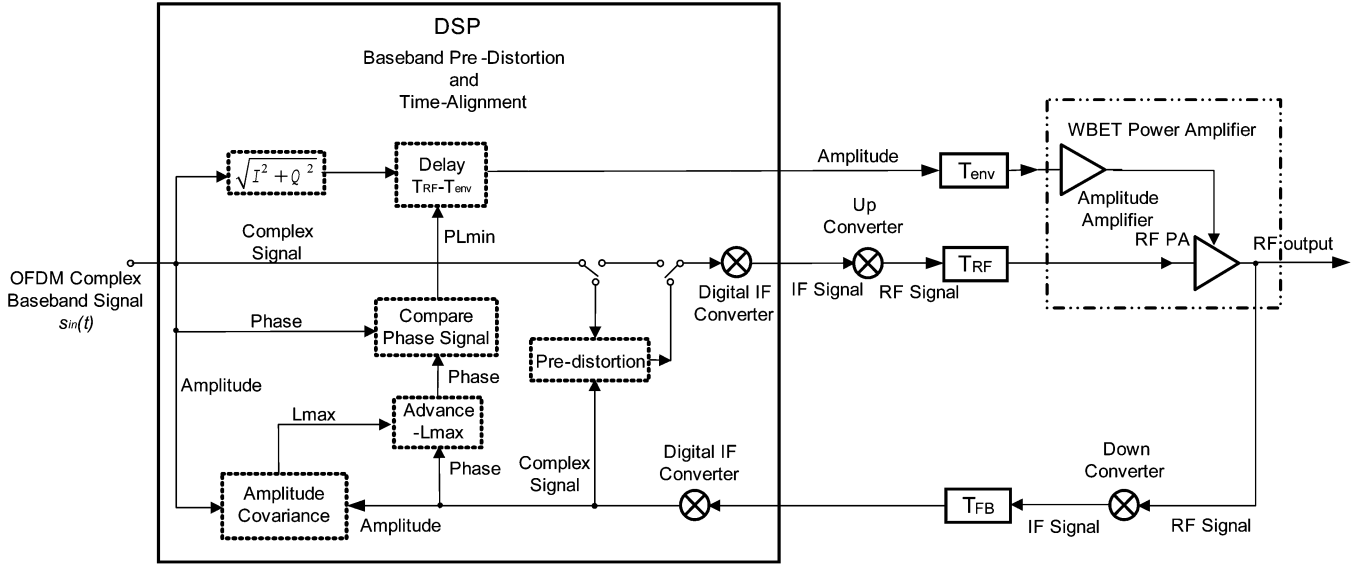


Fig. 3. Block diagram of WBET architecture with baseband predistortion and time-alignment algorithms.

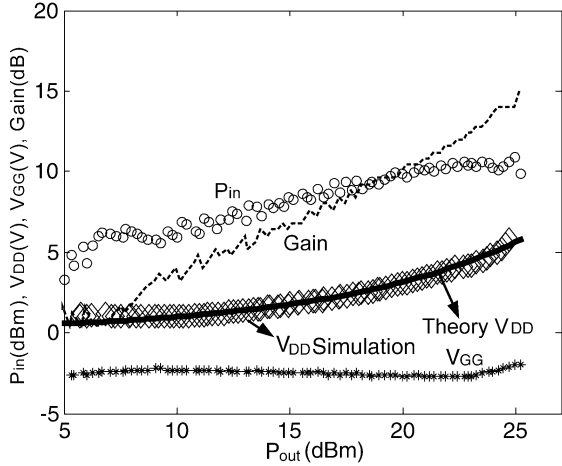


Fig. 4. Agilent ADS Simulation of the optimum (for maximum PAE) of V_{DD} , V_{GG} , and P_{in} for the 2.4-GHz GaAs MESFET class-AB PA of Section IV. The theoretical amplitude of the output signal is $(R_L P_{out})^{1/2}$.

B. ET System Time-Mismatch Analysis

A major concern with any supply control amplifier (either ET or EER) is the sensitivity of EVM and distortion to the time mismatch between the two signal paths. In order to study this effect, we used the Cann model for the amplifier [20]

$$v_o = \frac{g v_{in}}{\left[1 + \left(\frac{g}{L} |v_{in}|\right)^s\right]^{1/s}} \quad (3)$$

where g and L are functions of V_{DD} : g models the small-signal gain (in the PA linear region), s models the transition from the linear to the saturation region and is roughly independent of V_{DD} , and L models the saturated output value. [In this paper, the amplifier nonlinear behavior is modeled as AM-AM as (3). Compared to AM-AM, AM-PM can be neglected for small devices [13].]

In this case, v_o and v_{in} are the RF output and input voltages, respectively. Fig. 6 compares the v_{out} versus v_{in} for different V_{DD} by ADS simulation of the circuit described in Section IV

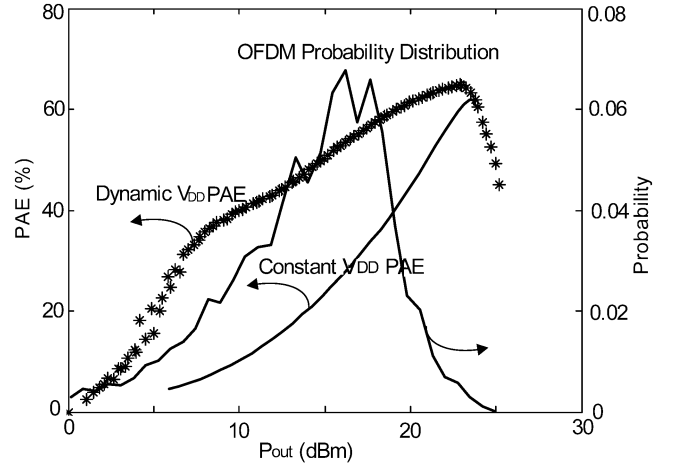


Fig. 5. Comparison of amplifiers of Fig. 4, where the drain bias is varied for maximum PAE (ET) and the drain bias is fixed at 4.4 V. The 802.11 g 64-QAM output amplitude power probability distribution is also shown.

TABLE II
SIMULATED PERFORMANCE OF FIXED V_{DD} CLASS-AB PA AND DIFFERENT ET CONFIGURATIONS AT $P_{out} = 12$ dBm

V_{DD} configuration	Case 1 Constant V_{DD}	Case 2 Signal envelope+ 0V	Case 3 Signal envelope + 0.5V
Gain (dB)	13.9	5.0	7.5
Drain η (%)	9.9	51	43.9
PAE (%)	9.5	34.9	36.1
EVM (rms%)	3.2	14.9	10.0

and the Cann model. With this model, the time-mismatch sensitivity can be analyzed.

The relative simplicity of the two-tone test signal eases the mathematical analysis of sensitivity of the EER and ET systems to the time mismatch (between the amplitude path and RF path). The two-tone modulated RF signal is defined by

$$s_{RF}(t) = \cos \omega_m t \cos \omega_c t \quad (4)$$

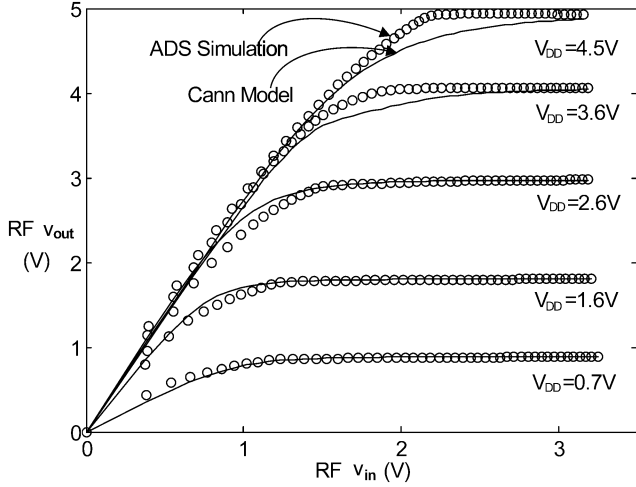


Fig. 6. Comparison of ADS simulation and Cann model of the GaAs MESFET PA of Section IV. A least-squares fit to the simulation data provides $g \approx 1.24 + 0.38V_{DD}$, $L \approx 0.09 + 1.15V_{DD}$, and $s \approx 5$.

where ω_m is baseband modulation frequency and ω_c is the RF carrier frequency.

Thus, the baseband signal of the two-tone RF signal is

$$s_{BB}(t) = \cos \omega_m t = A(t) \cdot e^{j\varphi(t)} \quad (5)$$

where the amplitude and phase signals are

$$A_{in}(t) = |\cos(\omega_m t)| \quad (6a)$$

$$\varphi_{in}(t) = \frac{\pi}{2} [1 - c(\omega_m t)]. \quad (6b)$$

$c(\omega_m t)$ is a square wave with a value of $+1$ or -1 with the same period as the modulation frequency. Expansion of the amplitude signal as a Fourier series produces

$$A(t) = a_0 + \sum_{n=2,4,6,\dots} a_n \cos(n\omega_m t) \quad (7)$$

where

$$a_0 = \frac{2}{\pi} \quad a_n = \frac{4(-1)^{(n-2)/2}}{\pi(n^2-1)}, \quad n = 2, 4, 6, \dots \quad (8)$$

If the time mismatch between the baseband amplitude and the RF phase path is τ for an EER system, then $A_{out}(t) = A_{in}(t - \tau)$, $\varphi_{out}(t) = \varphi_{in}(t)$ and, therefore,

$$s_{BB,out}(t) = A_{in}(t - \tau) \cdot e^{j\varphi_{in}(t)}. \quad (9)$$

Fig. 7 shows the simulated EER amplitude signal, phase signal, distorted output baseband signal, and error signal for a two-tone input with a time mismatch of 2.5 ns. The distorted output baseband signal indicates that, even for the ideal EER system, a time mismatch between the amplitude and phase produces error and intermodulation distortion. According to Raab [21] and Su and McFarland [10], for small delay, the

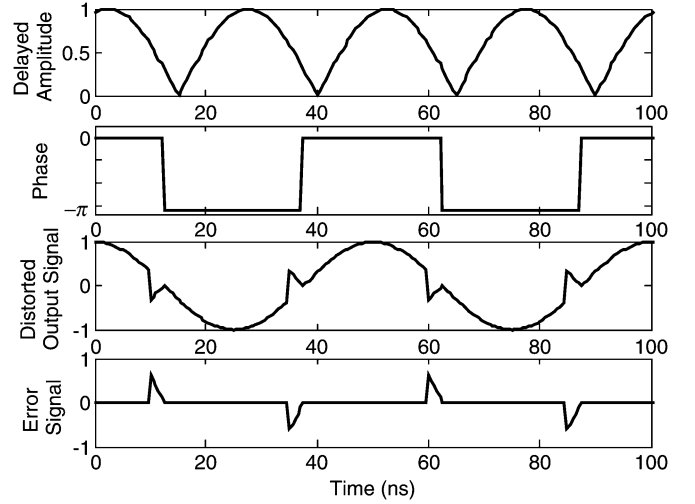


Fig. 7. Simulated two-tone EER system with time mismatch between baseband amplitude and RF phase. The modulation frequency is 20 MHz, and the baseband amplitude path time delay is 2.5 ns.

magnitude of the intermodulation distortion introduced by the time mismatch for a two-tone signal is

$$\text{IMD} \approx \left(\frac{2}{\pi}\right) (B_{RF}\tau)^2 \quad (10)$$

where B_{RF} is the bandwidth of the two-tone signal: $B_{RF} = 2\omega_m/2\pi$, and τ is the time mismatch between the baseband amplitude and RF phase.

By contrast, the output envelope of the WBET system is [from (3)]

$$A_{out}(t) = \frac{g(V_{DD}(t)) \cdot A_{in}(t)}{\left[1 + \left(\frac{g(V_{DD}(t))}{L(V_{DD}(t))} |A_{in}(t)|\right)^s\right]^{1/s}} \quad (11)$$

where $V_{DD}(t)$ is the dynamic drain voltage and it is a linear time-delayed function of the input envelope signal, i.e.,

$$V_{DD}(t) = V_{min} + kA_{in}(t - \tau). \quad (12)$$

The quantities $g(V_{DD})$ and $L(V_{DD})$ are functions of dynamic drain voltage V_{DD} (extracted in Fig. 6) as

$$g(V_{DD}) = g_0 + g_1 \cdot V_{DD} \quad (13a)$$

$$L(V_{DD}) = L_0 + L_1 \cdot V_{DD}. \quad (13b)$$

Since the WBET amplifier is nonlinear, predistortion is implemented in our proposed system. To focus on the distortion caused by the time mismatch and the resulting nonlinear limiting behavior, we assume that the predistortion is ideal, and any intermodulation and harmonic products generated by the nonlinearity of (11) will therefore be eliminated. However, nonlinear distortion is then re-introduced due to the time mismatch

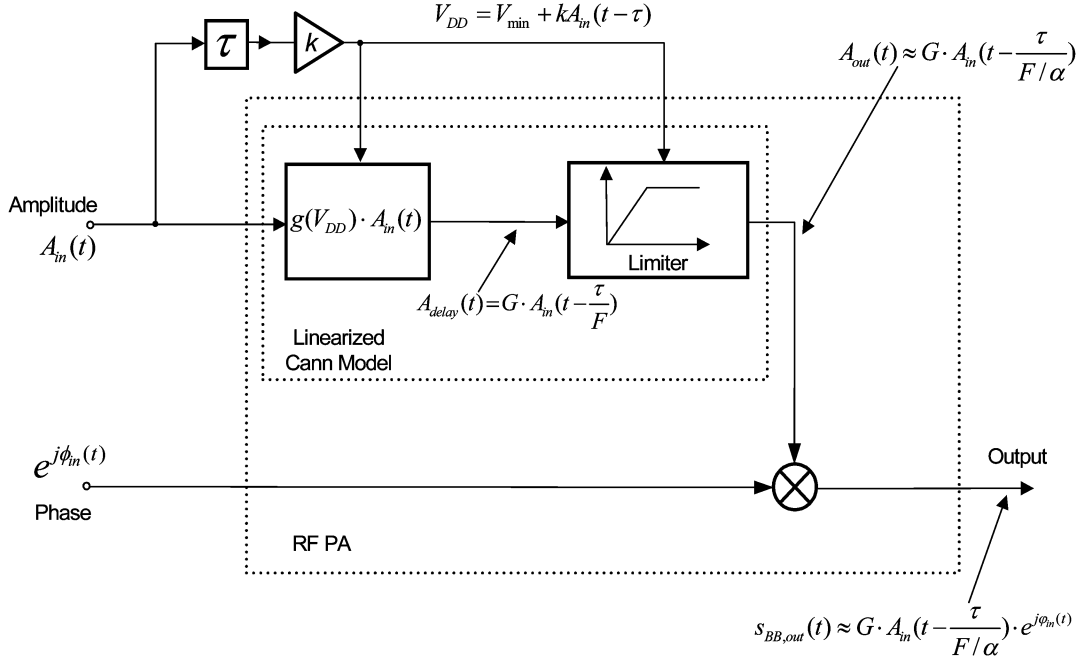


Fig. 8. Simplified ET system block diagram. The time mismatch between the baseband amplitude and RF amplitude/phase is τ .

of the amplitude and RF signals. As a result of the predistortion, the Cann model parameter s approaches infinity, and the denominator of (11) becomes a “hard limiter,” i.e., s

$$A_{out}(t) = \begin{cases} g(V_{DD}(t)) \cdot A_{in}(t), & g(V_{DD}(t))A_{in}(t) \leq L(V_{DD}(t)) \\ L(V_{DD}(t)), & g(V_{DD}(t))A_{in}(t) > L(V_{DD}(t)) \end{cases} \quad (14)$$

By calculating the linear delayed amplitude signal *before hard limiting* and then limiting the resulting signal as shown in Fig. 8, the output amplitude signal is shown in Fig. 9.

Prior to hard limiting, the amplitude of the RF output signal is

$$A_{delay}(t) = g(V_{DD}(t)) \cdot A_{in}(t). \quad (15)$$

Substituting (12) and (13a) into (15), the amplitude of the RF output signal is

$$\begin{aligned} A_{delay}(t) &= g_0 A_{in}(t) + g_1 A_{in}(t) \cdot [V_{min} + kA_{in}(t - \tau)] \\ &= (g_0 + g_1 V_{min})A_{in}(t) + g_1 k A_{in}(t)A_{in}(t - \tau). \end{aligned} \quad (16)$$

Note that in (16) the delayed magnitude signal $A_{delay}(t)$ is a nonlinear function of $A_{in}(t)$: the multiplication of $A_{in}(t)A_{in}(t - \tau)$ will generate intermodulation products. However, the predistortion will eliminate those nonlinear terms, leaving a remaining linear *but delayed* result.

The multiplication of $A_{in}(t)A_{in}(t - \tau)$ is described as [from (7)]

$$\begin{aligned} A_{in}(t)A_{in}(t - \tau) &= \left(a_0 + \sum_{n=2,4,6,\dots} a_n \cos(n\omega_m t) \right) \\ &\quad \cdot \left(a_0 + \sum_{n=2,4,6,\dots} a_n \cos(n\omega_m(t - \tau)) \right). \end{aligned} \quad (17)$$

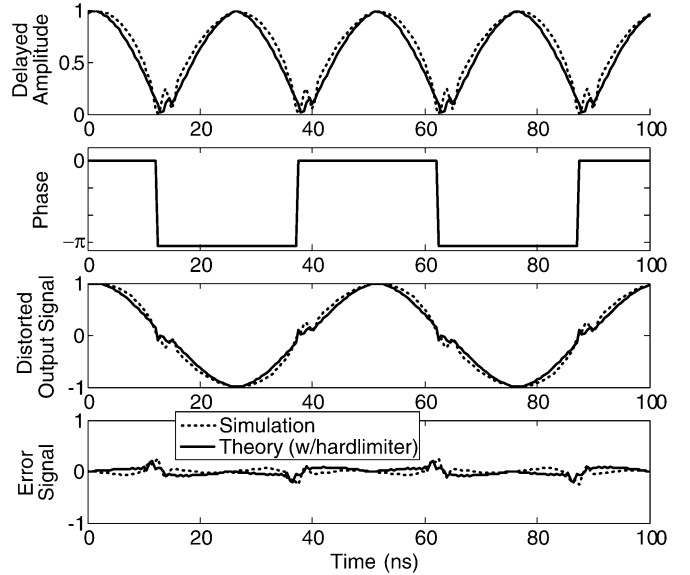


Fig. 9. Two-tone ET system with time mismatch between baseband amplitude and RF amplitude/phase. The modulation frequency is 20 MHz, and the baseband amplitude path time delay is 2.5 ns.

From the above, the linear product of the multiplication is

$$DC + a_0 \sum_{n=2,4,6,\dots} a_n [\cos(n\omega_m t) + \cos(n\omega_m(t - \tau))] \quad (18)$$

where DC represents the sum of all of the dc components resulting from the mismatch, and the nonlinear part is

$$\sum_{n=2,4,6,\dots} a_n \cos(n\omega_m t) \cdot \sum_{k=2,4,6,\dots} a_k \cos(k\omega_m(t - \tau)). \quad (19)$$

Adding (18) to (16) yields

$$\begin{aligned}
 A_{\text{delay}}(t) &= \text{DC} + (g_0 + g_1 V_{\min}) \sum_{n=2,4,6,\dots} a_n \cos(n\omega_m t) \\
 &\quad + g_1 k a_0 \sum_{n=2,4,6,\dots} a_n [\cos(n\omega_m t) + \cos(n\omega_m(t - \tau))] \\
 &= \text{DC} + \sum_{n=2,4,6,\dots} (g_0 + g_1 V_{\min} + g_1 k a_0 + g_1 k a_0 \cos n\omega_m \tau) \\
 &\quad \cdot a_n \cos(n\omega_m t) \\
 &\quad + \sum_{n=2,4,6,\dots} g_1 k a_0 \sin n\omega_m \tau \cdot a_n \sin(n\omega_m t) \\
 &= \text{DC} + \sum_{n=2,4,6,\dots} c'_n \cdot a_n \cos(n\omega_m(t - \tau_{\text{eff}})) \quad (20)
 \end{aligned}$$

where

$$c'_n = \sqrt{c_n^2 + d_n^2} \quad (21a)$$

$$c_n = g_0 + g_1 V_{\min} + g_1 k a_0 + g_1 k a_0 \cdot \cos n\omega_m \tau \quad (21b)$$

$$d_n = a_0 g_1 k \cdot \sin n\omega_m \tau \quad (21c)$$

$$\tau_{\text{eff}} = \frac{1}{n\omega_m} \tan^{-1} \left(\frac{d_n}{c_n} \right). \quad (21d)$$

Assuming the time mismatch τ is very small

$$\tau_{\text{eff}} \approx \frac{a_0 g_1 k}{g_0 + g_1 V_{\min} + g_1 k a_0 + g_1 k a_0} \cdot \tau = \frac{\tau}{F} \quad (22)$$

where the factor F represents the *desensitization factor* of the time mismatch in an ET system, i.e.,

$$F = \frac{g_0 + g_1 V_{\min} + 2g_1 k a_0}{a_0 g_1 k} \approx 2 + \frac{g_0}{a_0 g_1 k} \quad (23)$$

where $g_1 V_{\min}$ is small (for this example, $g_0 = 1.24$, $g_1 = 0.38$, $V_{\min} = 0.37$). By comparison, the value of F for an EER system is unity and the value of the desensitization factor F for an ET system is always greater than two.

From (21), c'_n represents a linear amplification of the original signal and therefore

$$A_{\text{delay}}(t) = G \cdot A_{\text{in}} \left(t - \frac{\tau}{F} \right) \quad (24)$$

where G represents the linear gain between the input and output magnitude signals

$$G = c'_n = \sqrt{c_n^2 + d_n^2} \approx g_0 + 2g_1 k a_0. \quad (25)$$

Limiting may then occur if there is a significant time mismatch between the baseband amplitude signal and the RF signal. This effect is shown in Figs. 9 and 10, where the mismatch between the RF amplitude/phase input and the baseband amplitude

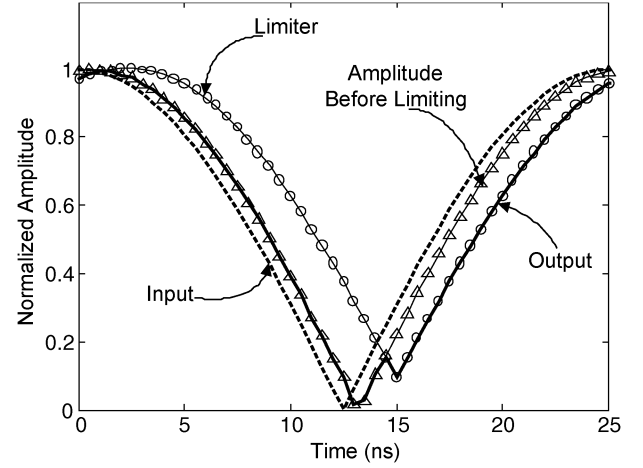


Fig. 10. Simulation of two-tone ET amplifier with time-delay mismatch. Note the distortion in the output amplitude due to the time mismatch between the baseband amplitude and RF amplitude signals and the limiting action of the amplifier. The baseband amplitude path time delay is 2.5 ns.

amplifier leads to severe distortion. This can be modeled by substituting (12), (13b), (15), and (24) into (14). Then, the *normalized* ET output amplitude signal is given by the following:

$$\begin{aligned}
 A_{\text{out_norm}}(t) &= \begin{cases} A_{\text{in}} \left(t - \frac{\tau}{F} \right), \\ \text{if } A_{\text{in}} \left(t - \frac{\tau}{F} \right) \leq \frac{L_0 + L_1 V_{\min} + L_1 k A_{\text{in}}(t - \tau)}{G} \\ \frac{L_0 + L_1 V_{\min} + L_1 k A_{\text{in}}(t - \tau)}{G}, \\ \text{if } A_{\text{in}} \left(t - \frac{\tau}{F} \right) > \frac{L_0 + L_1 V_{\min} + L_1 k A_{\text{in}}(t - \tau)}{G}. \end{cases} \quad (26)
 \end{aligned}$$

As an example, we extracted the Cann parameters from the ADS simulations of the circuit described in the Section IV (refer to Figs. 4, 6, and 18) and extracted $g_0 = 1.24$, $g_1 = 0.38$, $V_{\min} = 0.37$, $k = 2$, $L_0 = 0.1$, and $L_1 = 1.15$. Substituting the above parameters into (23) and (25), we obtained $F = 4.5$, $G = 2.2$, and $L_1 k / G = 1.05$, and the *normalized* ET output amplitude is given by the following:

$$\begin{aligned}
 A_{\text{out_norm}}(t) &= \begin{cases} A_{\text{in}} \left(t - \frac{\tau}{F} \right), \\ \text{if } A_{\text{in}} \left(t - \frac{\tau}{F} \right) \leq 0.2 + 1.05 A_{\text{in}}(t - \tau) \\ 0.2 + 1.05 A_{\text{in}}(t - \tau), \\ \text{if } A_{\text{in}} \left(t - \frac{\tau}{F} \right) > 0.2 + 1.05 A_{\text{in}}(t - \tau). \end{cases} \quad (27)
 \end{aligned}$$

Fig. 9 also shows the comparison between the theoretical calculation and Cann model simulation, and the two agree well. Fig. 10 shows the RF input amplitude signal, the *normalized* linear delayed amplitude signal after amplification but before

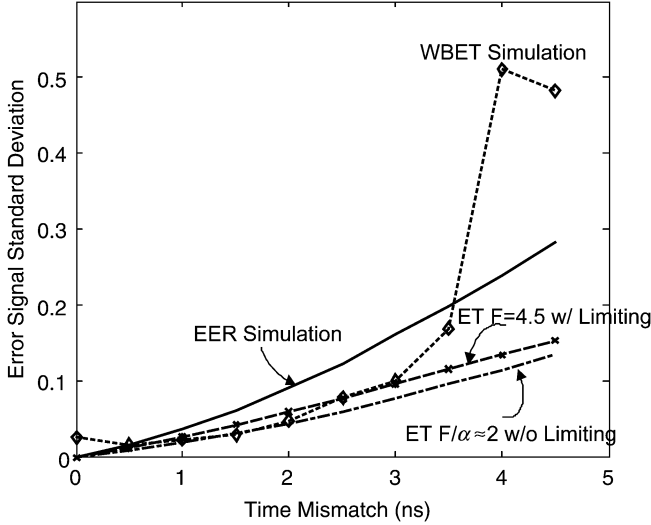


Fig. 11. Two-tone error-signal standard deviation versus time mismatch for EER and ET systems. As predicted in (27) and (28), the simulation of the Cann model agrees with the theory for $F = 4.5$ (27) with hard limiting and the theory for $F/\alpha = 2$ (28) without hard limiting. Note that the EER is more sensitive to path-mismatch effects than the ET system. The simulation results deviate from the theory at high mismatch values due to the high time mismatch for the higher order harmonic components and nonideal predistortion.

limiting (refer to Fig. 8), the *normalized* limiting signal (the delayed amplitude amplifier output with minimum voltage offset) $L(V_{DD}(t))/G$, and the *normalized* output RF amplitude signal after limiting. From Fig. 10, during approximately half of the cycle, the output amplitude signal is the same as the linear delayed amplitude signal, which has a delay of τ/F as shown earlier. During the other half of the period, the output is limited by the drain amplitude signal, which has a delay of τ . Thus, the *normalized* output amplitude signal can be approximated by a simple expression, i.e.,

$$A_{\text{out_norm}}(t) \approx A_{\text{in}} \left(t - \frac{\tau}{F} \right) \quad (28)$$

where α is the “*limiting effect factor*” and F/α is approximately two for the two-tone signal, since the amplitude signal is limited by the envelope delay during half the period only.

Finally, from (28), the complex *normalized* baseband output signal is

$$s_{\text{BB,out_norm}}(t) \approx A_{\text{in}} \left(t - \frac{\tau}{F} \right) \cdot e^{j\varphi_{\text{in}}(t)}. \quad (29)$$

Comparing (29) (the ET output signal) with (9) (the EER output signal), the time mismatch between the baseband amplitude path and RF path for ET system is decreased (desensitized) by a factor of F/α , thus the IMD magnitude is decreased by a factor of $(F/\alpha)^2$ compared to (10) for EER. Fig. 11 compares the error-signal standard deviation between EER simulation, ET Cann simulation, the theoretical calculation with limiting effect by using (26), and the equivalent theoretical calculation by using (28) for a two-tone test signal. The ET simulation agrees with the theoretical analysis very well when the time mismatch is less than three nanoseconds. Beyond three nanoseconds, due to

the nonideal predistortion, the simulation shows a larger error-signal standard deviation than the theoretical calculations.

Compared with a two-tone signal, the OFDM signal has a higher PAR, which implies a lower normalized dc component a_0 for a given output power. From (23), a lower a_0 leads to a higher F . For example, using the amplifier parameters discussed previously, an OFDM 802.11 g signal has a normalized a_0 of 0.3 and a resulting $F = 7.5$. Such a large F leads to an effective factor F/α of approximately two for any ET system. From Fig. 10, the larger the value of F is, the closer the linear delayed amplitude signal approaches to the input RF amplitude signal, and the average between the τ/F and τ will be closer to the average of τ and zero (i.e., $\tau/2$).

For example, suppose F is infinite, then the linear delayed amplitude signal will overlay with the original RF input amplitude signal. From Fig. 10, during half of the cycle, the output amplitude signal is the same as the RF input amplitude signal, which has a delay of zero, during the other half of the time, the output is limited by the drain amplitude signal, which has a delay of τ . Thus, the normalized output envelope signal is delayed by $\tau/2$.

To summarize the results of this section, we have derived an expression for the “effective” time-alignment mismatch between the amplitude (drain) and RF (gate) signals of an ET amplifier, based on the Cann nonlinear model, assuming ideal predistortion. It was demonstrated that the ET amplifier is significantly less sensitive than the traditional EER amplifier to this misalignment—a crucial benefit for wide-bandwidth operation. These results agree well with detailed simulation results, as well as measured results (refer to Section IV), and can be used to estimate the resulting errors in a complete system. Section III will suggest an algorithm to precisely time align the amplitude and RF signals.

III. ADAPTIVE TIME-ALIGNMENT ALGORITHM FOR ENVELOPE TRACKING SYSTEM

As shown in the previous section, time alignment is required for the ET system to align the baseband amplitude path and RF path, especially for wideband OFDM signals. An adaptive real-time time-alignment technique is needed because of inevitable environmental variations. A time alignment of better than 2 ns (refer to Section IV) is required to make the EVM lower than 3% for an OFDM 802.11 a/g signal. In this case, the signal bandwidth is approximately 20 MHz, and, with a data converter sample rate of approximately 100 MHz, linear interpolation will be required to achieve the necessary subsample delay accuracy.

Referring to Fig. 3, we first calculate the covariance between the original amplitude signal and the down converted feedback signal. The covariance is calculated for amplitudes of s_{in} and s_{out} as

$$C_{A_{\text{in}},A_{\text{out}}}(L) = E[(A_{\text{in}}(t+L) - \mu_{A_{\text{in}}}) \cdot (A_{\text{out}}(t) - \mu_{A_{\text{out}}})] \quad (30)$$

where E is the expectation operator, $\mu_{A_{\text{in}}}$ and $\mu_{A_{\text{out}}}$ represent the mean value of the input amplitude signal A_{in} and output amplitude signal A_{out} . L is the time offset of the covariance (note that this L is different from the Cann model parameter “ L ” in the

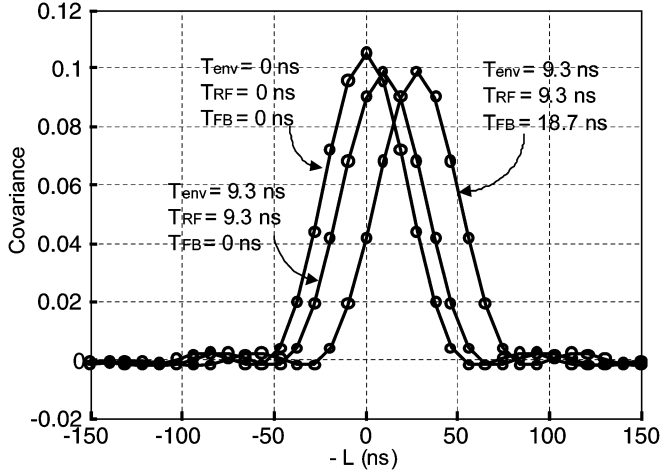


Fig. 12. Simulated covariance of RF input amplitude A_{in} and RF output amplitude A_{out} [refer to (30)] for different values of T_{env} , T_{RF} , and T_{FB} for OFDM 802.11 g signal. Note that the peak of the covariance occurs at the sum of T_{FB} and a weighed average of T_{env} and T_{RF} .

previous section), and L_{max} is the time offset corresponding to the maximum covariance. For example, Fig. 12 shows the simulated covariance of A_{in} and A_{out} for different values of T_{env} , T_{RF} , and T_{FB} for an 802.11 a/g OFDM signal applied to the ET amplifier described in the previous section.¹ This information can be used to compensate the loop delay of the transmitter path plus the down-converted feedback path.

Fig. 13 shows the simulated EVM [see Fig. 13(a)] and L_{max} [see Fig. 13(b)] versus T_{env} for different values of T_{RF} when T_{FB} is zero. As expected, the minimum in the EVM occurs when T_{env} is equal to T_{RF} . From Fig. 13, in the case where T_{FB} equals zero,

$$L_{max} \approx -\frac{T_{RF} + T_{env}}{2}. \quad (31)$$

However, in practice, the practical feedback path time delay T_{FB} is not zero, due to the various filters in the RF path and other components. Fig. 14 shows the simulated L_{max} and EVM versus T_{env} for different values of T_{RF} and T_{FB} . From Fig. 14, the function of L_{max} versus T_{env} , T_{RF} , and T_{FB} is

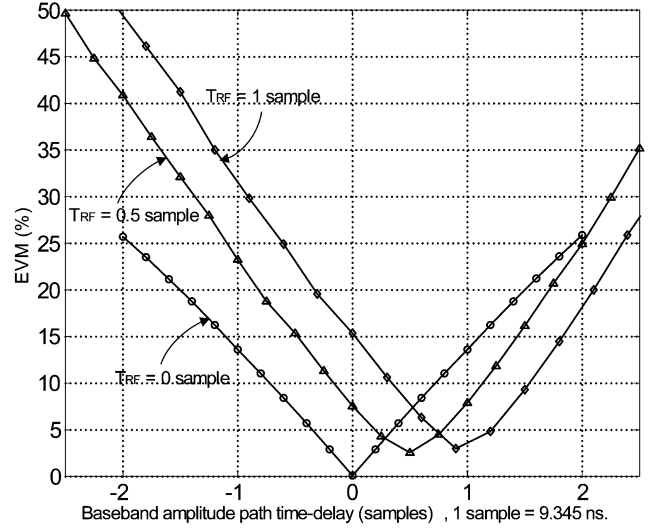
$$L_{max} \approx -\left(T_{FB} + \frac{T_{RF} + T_{env}}{2}\right) \quad (32)$$

and the general expression for L_{max} is

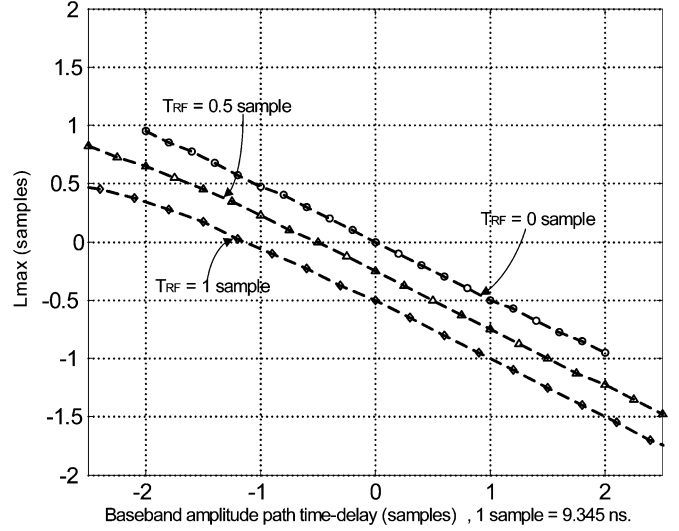
$$L_{max} \approx -\left(T_{FB} + T_{RF} + \frac{T_{env} - T_{RF}}{\frac{F}{\alpha}}\right) \quad (33)$$

which represents the weighting of the loop delay of the transmitter path plus the down-converted feedback path when applied to the ET amplifier. This agrees with the previous section

¹All the following simulations and measurements are with an 802.11 g OFDM signal at 54-Mb/s data rate.



(a)



(b)

Fig. 13. (a) Simulated EVM and (b) L_{max} (T_{FB} is zero). $L_{max} \approx -T_{env}/2$ (for $T_{RF} = 0$); $L_{max} \approx -1/4 - T_{env}/2$ (for $T_{RF} = 0.5$ samples); $L_{max} \approx -1/2 - T_{env}/2$ (for $T_{RF} = 1$ samples).

analysis that the effective amplitude delay of the ET system is approximately the average of the time mismatch between the baseband amplitude path delay and RF path delay (i.e, F/α is approximately two).

Given that we can determine L_{max} by experimentally measuring the maximum of the covariance, we then compensate the down-converted feedback phase signal for the loop delay by advancing the feedback phase signal $\varphi_{fb}(t) = \varphi_{fb}(t - L_{max})$. Before this compensation, from Fig. 3, the feedback phase signal is $\varphi_{fb}(t) = \varphi_{in}(t - T_{RF} - T_{FB})$. After this loop delay compensation is completed, the feedback phase signal becomes

$$\begin{aligned} \varphi_{fb}(t) &= \varphi_{in}(t - T_{RF} - T_{FB} - L_{max}) \\ &= \varphi_{in}\left(t - \frac{T_{RF} - T_{env}}{\frac{F}{\alpha}}\right). \end{aligned} \quad (34)$$

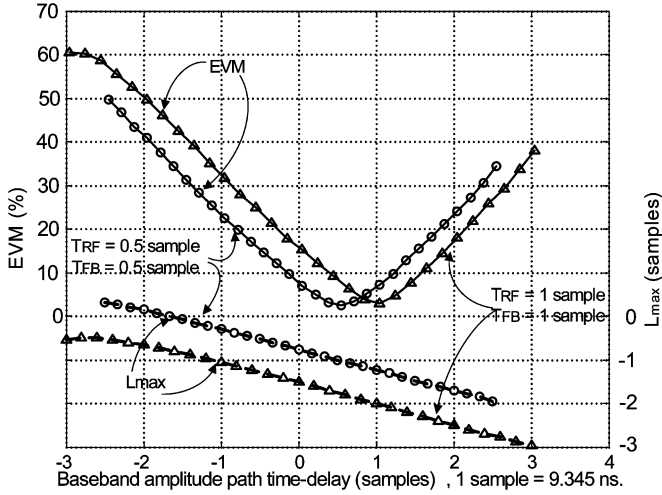


Fig. 14. Simulated EVM and L_{\max} for variations in T_{FB} . Note that the minimum EVM occurs when $T_{\text{env}} = T_{\text{RF}}$, and $L_{\max} = -T_{\text{FB}} - (T_{\text{RF}} + T_{\text{env}})/2$.

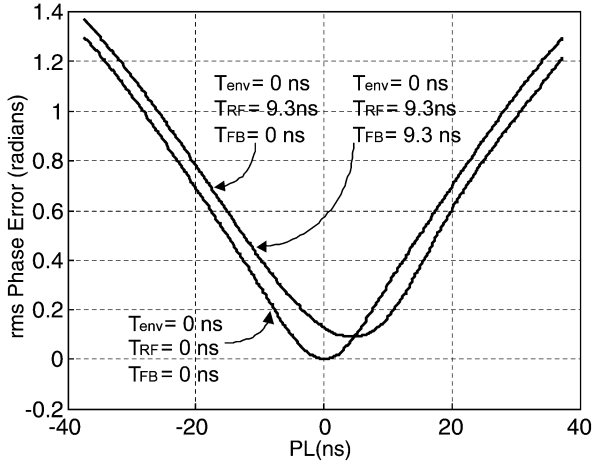


Fig. 15. Simulated rms phase error for different values of T_{env} , T_{RF} , and T_{FB} . Note that the curve of $T_{\text{env}} = 0$, $T_{\text{RF}} = 9.3$ ns and $T_{\text{FB}} = 0$ overlay with the curve of $T_{\text{env}} = 0$, $T_{\text{RF}} = 9.3$ ns, and $T_{\text{FB}} = 9.3$ ns. Therefore, the phase error is relatively insensitive to T_{FB} , which agrees with (34).

The rms value of the difference between the input and output phase signal (phase error signal) after loop delay compensation is

$$e(t, PL) = \varphi_{\text{in}}(t) - \varphi_{\text{fb}}(t - PL) \\ = \varphi_{\text{in}}(t) - \varphi_{\text{in}}\left(t - \frac{T_{\text{RF}} - T_{\text{env}}}{f} - PL\right) \quad (35a)$$

$$C_{\varphi_{\text{fb}}, \varphi_{\text{out}}}(PL) = \sqrt{\frac{1}{T} \int (e(t, PL) - \overline{e(t, PL)})^2} \quad (35b)$$

where PL is the time offset and $\overline{e(t, PL)}$ represents the mean value of the error signal.

Fig. 15 shows the simulated error signal standard deviation versus PL for different T_{env} , T_{RF} , and T_{FB} . PL_{\min} is the value

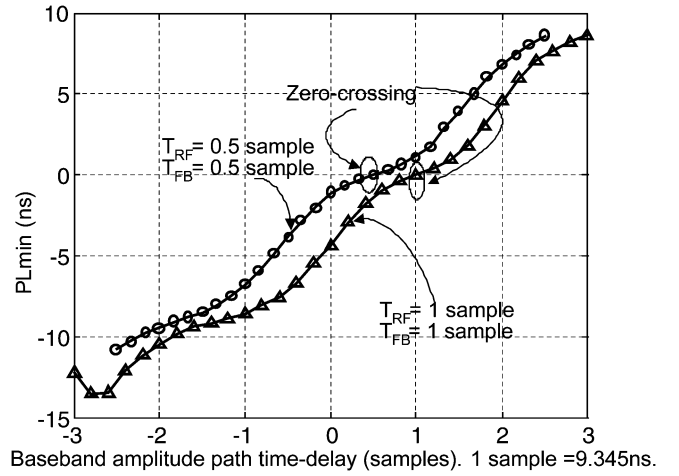


Fig. 16. Simulated value of PL_{\min} as a function of T_{env} . The value of T_{env} where PL_{\min} crosses zero is equal to T_{RF} , and its value is independent of T_{FB} . The average slope is 0.5 (note that the y axis one-step unit is 5 ns, the x axis one-step unit is one sample, which is 9.345 ns).

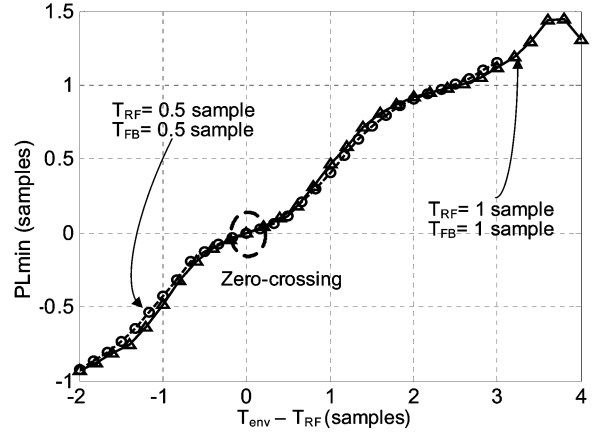


Fig. 17. Simulated value of PL_{\min} versus the time mismatch between T_{RF} and T_{env} . Note that this is independent of T_{FB} .

of PL corresponding to the minimum rms error signal. From (34) and (35), and Fig. 15,

$$PL_{\min} \approx \frac{T_{\text{env}} - T_{\text{RF}}}{\frac{F}{\alpha}} \quad (36)$$

Fig. 16 shows the simulated value of PL_{\min} as a function of T_{env} for different values of T_{RF} and T_{FB} . Note that—as expected— PL_{\min} is equal to zero when T_{env} is equal to T_{RF} , and this result is independent of T_{FB} .

Another way of looking at this result is shown in Fig. 17, where the simulated value of PL_{\min} versus $(T_{\text{env}} - T_{\text{RF}})$ is plotted for different values of T_{FB} and T_{RF} . Note that the average slope of PL_{\min} versus $(T_{\text{env}} - T_{\text{RF}})$ is approximately 0.5, which agrees well with (36) when $F/\alpha = 2$. From Figs. 15–17, we can see that PL_{\min} is only dependent on the time difference between T_{RF} and T_{env} , and it is independent of the values of T_{env} , T_{RF} , and T_{FB} . Thus, the time alignment scheme that we have outlined here is very robust to the inevitable variations in these parameters.

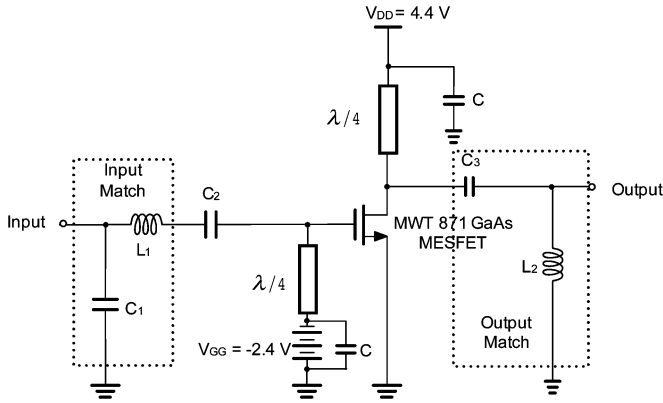


Fig. 18. GaAs MESFET Class-AB RFPA schematic diagram.

IV. EXPERIMENTAL RESULTS

An MWT-871 GaAs MESFET transistor [22], was used to implement the Class-AB RF PA,² as shown in Fig. 18. Quarter-wave transmission lines are used at the input and output to short the even harmonics. For a 2.4-GHz single-tone test, the measured gain is 13 dB and the peak PAE is 52% at an output power of 23 dBm.

The tested ET system includes a wide-band high-efficiency envelope amplifier [22] and the Class-AB RF PA. The WLAN baseband OFDM signal is upconverted digitally to an IF of 26.88 MHz at a sample rate of 107.52 MHz. Then, by a Xilinx FPGA running at 200 MHz and a dual-port RAM, the digital IF signal, as well as the amplitude signal, are output to two 107.52-MHz 14-b digital-to-analog converters (DACs). The IF signal is then upconverted to 2.4 GHz and amplified by the ET amplifier. The output RF signal is downconverted to an IF of 26.88 MHz and digitized by a 107.52-MHz 12-b analog-to-digital converter (ADC) and a buffer (a logic analyzer). In the measurement, the overhead associated with the extra dc power dissipation of the digital logic for the predistortion and signal conversion is not included. It is expected that these terms will play an increasingly less significant role in future digital communications as VLSI technology continues to advance.

Since the ET system has inherent nonlinearity associated with the gain variation as the drain voltage changes, baseband predistortion is implemented to improve the system linearity [22]. An inverse nonlinearity is created in the baseband predistortion prior to upconversion based on the measured AM-AM and AM-PM functions.

Fig. 19 shows the comparison between the theoretical calculation using (28), simulation, and measurement of the EVM of a WBET amplifier for an OFDM 802.11 g signal. The agreement between the experimental data, the simulations, and calculations, is excellent. From Fig. 19, the EVM is a linear function of the time mismatch τ i.e.,

$$EVM = \beta \cdot \tau \tag{37}$$

²Microwave Technology, Fremont, CA. [Online]. Available: www.mwtinc.com

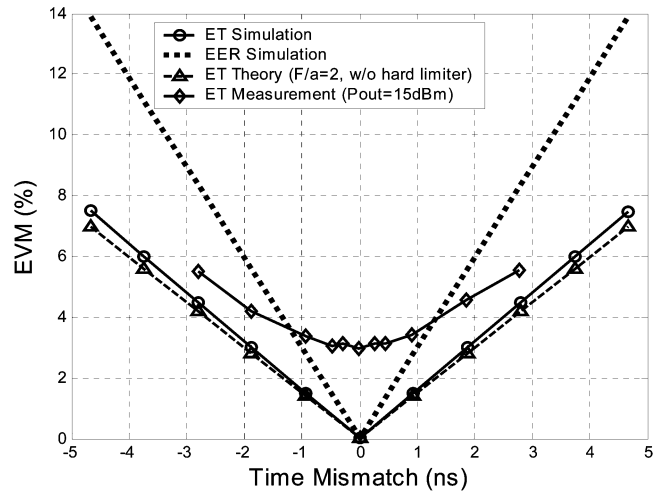


Fig. 19. Simulation and measurement of EVM versus baseband amplitude path time delay for ET and EER systems for an 802.11 g signal. The measurement is made with the GaAs MESFET RF PA with $P_{out} = 15$ dBm. Note that the measured slope of the EVM versus time mismatch agrees well with the theory. The measured minimum error floor of 3% is due to other impairments in the RF path unrelated to the time mismatch.

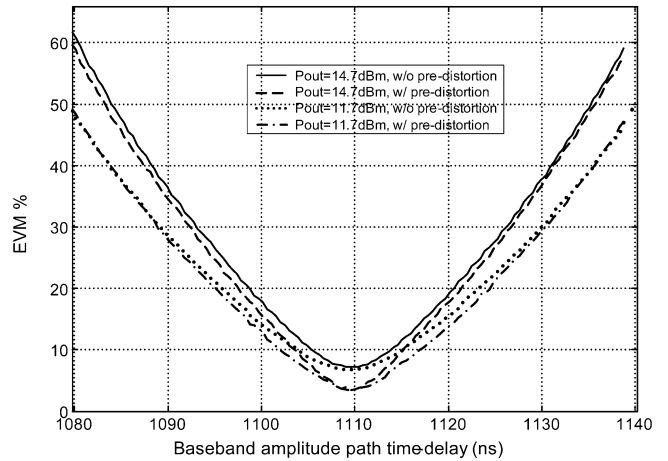


Fig. 20. Measured EVM versus baseband amplitude path time delay T_{env} for WLAN 802.11 g application (data rate 54 Mp/s). The minimum EVM indicates that the time difference between the RF path and baseband amplitude path is approximately 1110 ns.

where the proportionality factor β for EER is roughly six, and, for ET, since the effective delay is half of the time mismatch between the envelope path and RF path, the proportionality factor is only three. Compared with the ET system, the EER system's EVM is approximately twice as sensitive to the time mismatch. The measurement results agree well with the results predicted in (28).

Figs. 20 and 21 show the measured EVM and PL_{min} versus the time mismatch between the RF path and baseband amplitude path before and after predistortion. Note that the average slope of PL_{min} versus the time mismatch is approximately 0.5 for the time mismatch ± 20 ns around 1110 ns, which agrees well with the theory of $F/\alpha = 2$ for an 802.11 g signal [refer to (36)]. Comparing Fig. 21 with Fig. 17, the measurement results agree with the simulation and theory very well, and the zero crossing

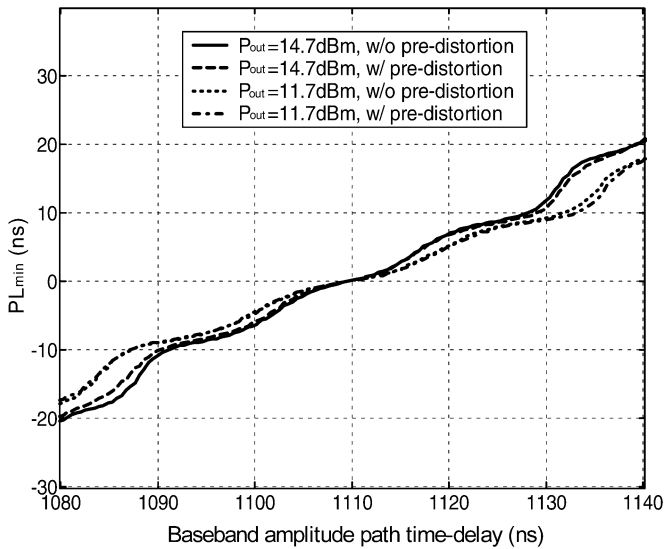


Fig. 21. Measured PL_{\min} versus baseband amplitude path time delay T_{env} for WLAN 802.11 g application (data rate 54 Mp/s). The zero-crossing of PL_{\min} indicates that the time difference between the baseband amplitude path and RF amplitude/phase path is approximately 1110 ns, which agrees well with the result from Fig. 20. Note that the average slope of PL_{\min} versus the time mismatch is approximately 0.5, which agrees well with the theory of $F/\alpha = 2$ for the 802.11 g signal [refer to (36)].

of PL_{\min} is independent of the output power. This demonstrates the accuracy of the time-alignment technique.

The peak drain efficiency of the *complete* amplifier (including the envelope amplifier and RF power amplifier, but not including the digital circuit power consumption) was 30% at an OFDM output power of 20 dBm for the Sirenza HFET PA,³ as reported in [22]. Compared with conventional linear Class-AB power amplifier, the efficiency is improved by more than a factor of two.

V. CONCLUSION

A general mathematical model was proposed to study the time-alignment requirement for the ET system. The time-mismatch sensitivity between the amplitude path and RF path was compared between the ET and EER systems. The simulation and measurement for the two-tone signal and WLAN OFDM signal generally verify the simple ET system model and the analysis. An adaptive time-alignment algorithm was developed for the ET system, and the simulation and measurement shows the fine time-alignment resolution could be smaller than 0.5 ns, satisfying the 802.11 g OFDM requirements.

ACKNOWLEDGMENT

The authors would like to acknowledge many valuable discussions and help with the hardware circuit design from A. Ojo, University of California at San Diego (UCSD), La Jolla, and Broadcom. The authors would also like to acknowledge many valuable discussions and MATLAB codes from Dr. D. Qiao and Dr. J. Jeong, both of UCSD. The authors wish to thank B.

Nelson, Sirenza Microdevices, Broomfield, CO, for the donation of the HFET SHF-0289 transistors. The authors also wish to thank the Microwave Technology Company, Fremont, CA, for the donation of the GaAs MESFET MWT-871 transistors.

REFERENCES

- [1] L. E. Larson, *RF and Microwave Circuit Design for Wireless Communications*. Boston, MA: Artech House, 1996.
- [2] H. Krauss, C. Bostian, and F. Raab, *Solid State Radio Engineering*. New York: Wiley, 1980.
- [3] S. C. Cripps, *RF Power Amplifiers for Wireless Communications*. Norwood, MA: Artech House, 1999.
- [4] P. B. Kennington, *High Linearity RF Amplifier Design*. Norwood, MA: Artech House, 2000.
- [5] F. H. Raab, P. Asbeck, S. Cripps, P. B. Kennington, Z. B. Popović, N. Potheary, J. F. Sevic, and N. O. Sokal, "Power amplifiers and transmitters for RF and microwave," *IEEE Trans. Microw. Theory Tech.*, vol. 50, no. 3, pp. 814–826, Mar. 2002.
- [6] *Part 11: Wireless LAN Medium Access Control (MAC) and Physical Layer Specifications*, IEEE Standard 802.11a/b/g/1999/1999/2003, 2003.
- [7] Agilent Technol., Palo Alto, CA, Agilent Applicat. Note AN 1380-4, 2003.
- [8] L. Kahn, "Single-sided transmission by envelope elimination and restoration," *Proc. IRE*, pp. 803–806, Jul. 1952.
- [9] R. H. Raab, B. E. Sigmon, R. G. Myers, and R. M. Jackson, "L-band transmitter using Kahn EER technique," *IEEE Trans. Microw. Theory Tech.*, vol. 46, no. 12, pp. 2220–2225, Dec. 1998.
- [10] D. Su and W. McFarland, "An IC for linearizing RF power amplifiers using envelope elimination and restoration," *IEEE J. Solid-State Circuits*, vol. 33, no. 12, pp. 2252–2258, Dec. 1998.
- [11] M. Iwamoto, A. Williams, P. Chen, A. G. Metzger, L. E. Larson, and P. M. Asbeck, "An extended Doherty amplifier with high efficiency over a wide power range," *IEEE Trans. Microw. Theory Tech.*, vol. 49, no. 12, pp. 2472–2479, Dec. 2001.
- [12] G. Hanington, P. Chen, P. M. Asbeck, and L. E. Larson, "High efficiency power amplifier using dynamic power-supply voltage for CDMA applications," *IEEE Trans. Microw. Theory Tech.*, vol. 47, no. 8, pp. 1471–1476, Aug. 1999.
- [13] J. Staudinger, B. Gilsdorf, D. Newman, G. Norris, G. Sadowiczak, R. Sherman, and T. Quach, "High efficiency CDMA power amplifier using dynamic envelope tracking technique," in *IEEE MTT-S Int. Microwave Symp. Dig.*, 2000, pp. 873–976.
- [14] B. Sahu and G. A. Rincon-Mora, "A high-efficiency linear RF power amplifier with power-tracking dynamically adaptive buck-boost supply," *IEEE Trans. Microw. Theory Tech.*, vol. 52, no. 1, pp. 112–120, Jan. 2004.
- [15] D. R. Anderson and W. H. Cantrell, "High efficiency high level modulator for use in dynamic envelope tracking CDMA RF power amplifiers," in *IEEE MTT-S Int. Microwave Symp. Dig.*, 2001, pp. 1509–1512.
- [16] X. Zhang, L. E. Larson, and P. M. Asbeck, *Design of Linear RF Outphasing Power Amplifiers*. Norwell, MA: Artech House, 2003.
- [17] A. A. M. Saleh, D. C. Cox, and D. C. Cox, "Improving the power added efficiency of FET amplifiers operating with varying-envelope signals," *IEEE Trans. Microw. Theory Tech.*, vol. MTT-31, no. 1, pp. 51–56, Jan. 1983.
- [18] K. Yang, G. I. Haddad, and J. R. East, "High-efficiency class-A power amplifiers with dual bias-control scheme," *IEEE Trans. Microw. Theory Tech.*, vol. 47, no. 8, pp. 1426–1432, Aug. 1999.
- [19] J. B. Groe and L. E. Larson, *CDMA Mobile Radio Design*. Norwell, MA: Artech House, 2000.
- [20] A. J. Cann, "Nonlinearity model with variable knee sharpness," *IEEE Trans. Aerosp. Electron. Syst.*, vol. AES-16, no. 6, pp. 874–877, Nov. 1980.
- [21] F. H. Raab, "Intermodulation distortion in Kahn-technique transmitters," *IEEE Trans. Microw. Theory Tech.*, vol. 44, no. 12, pp. 2273–2278, Dec. 1996.
- [22] F. Wang, A. Ojo, D. Kimball, P. M. Asbeck, and L. E. Larson, "Envelope tracking power amplifier with pre-distortion for WLAN 802.11 g," in *IEEE MTT-S Int. Microwave Symp. Dig.*, 2004, pp. 1543–1546.

³Sirenza Microdevices, Broomfield, CO. [Online]. Available: www.sirenza.com



Feipeng Wang (S'04) received the B.S. degree in electrical engineering from Xian Jiaotong University, Xian, China, in 1996, the M.S. degree in electrical engineering from the Chinese Academy of Sciences, Beijing, China, in 1999, and is currently working toward the Ph.D. degree in electrical engineering at the University of California at San Diego, La Jolla. His doctoral research concerns the design of high-efficiency linear ET power amplifiers for WLAN OFDM systems.

From 1997 to 1999, he was a Research Assistant with the Center for Space Science and Applied Research, Chinese Academy of Sciences. From 2000 to 2002, he was a Teaching Assistant with the University of Texas at Arlington. His research interests include RF and analog IC design for wireless communications.

Mr. Wang was the recipient of the Second-Place Award of the Best Student Paper presented at the 2004 IEEE Microwave Theory and Techniques Society (IEEE MTT-S) International Microwave Symposium (IMS). He was also the recipient of the Rudolph Hermann's Fellowship (2000–2001) and Texas Telecommunications Engineering Consortium Scholarship (TxTEC) (2001–2002) presented by the University of Texas at Arlington and the CAL(IT)2 Fellowship (2002–2003) presented by the University of California at San Diego.



Annie Hueiching Yang (S'02) received the B.S. degree in electrical engineering from the University of California at Irvine, in 2002, and the M.S. degree in electrical engineering from the University of California at San Diego, La Jolla, in 2004. Her M.S. thesis focused on the investigation and modeling of the EER and the ET systems for WLAN 802.11 a/g OFDM signals.

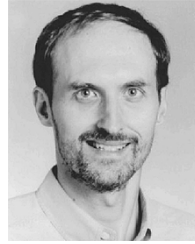
She is currently an RF Engineer with the Space and Naval Warfare System Center, San Diego, CA. From 2001 to 2002, she was an Undergraduate Student Researcher with the Integrated Nanosystems Research Facility, University of California at Irvine. From 2003 to 2004, she was a Teaching Assistant with the University of California at San Diego. She currently develops *S*-band high-efficiency class-E power amplifiers for transceiver application.



Donald F. Kimball (S'82–M'83) was born in Cleveland, OH, in 1959. He received the B.S.E.E. degree (*summa cum laude*) and M.S.E.E. degree from The Ohio State University, Columbus, in 1982 and 1983, respectively.

From 1983 to 1986, he was a TEMPEST Engineer with the Data General Corporation. From 1986 to 1994, he was an Electromagnetic Compatibility Engineer/Manager with Data Products New England. From 1994 to 1999, he was a Regulatory Product Approval Engineer/Manager with Qualcomm, Inc.

From 1999 to 2002, he was a Research and Technology Engineer/Manager with Ericsson, Inc. Since 2003, he has been a Principal Development Engineer with Cal(IT)2 with the University of California at San Diego, La Jolla. He holds four U.S. patents with two patents pending associated with high-power RF amplifiers (HPAs). His research interests include HPA EER techniques, switching HPAs, adaptive digital predistortion, memory effect inversion, mobile and portable wireless device battery management, and small electric-powered radio-controlled autonomous aircraft.

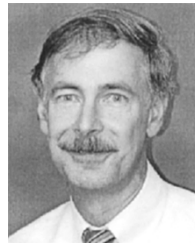


Lawrence E. Larson (S'82–M'86–SM'90–F'00) received the B.S. and M.Eng. degrees in electrical engineering from Cornell University, Ithaca, NY, in 1979 and 1980, respectively, and the Ph.D. degree in electrical engineering from the University of California at Los Angeles (UCLA), in 1986.

From 1980 to 1996, he was with Hughes Research Laboratories, Malibu, CA, where he directed the development of high-frequency microelectronics in GaAs, InP, Si/SiGe, and microelectromechanical systems (MEMS) technologies. In 1996, he joined

the faculty of the University of California at San Diego (UCSD), La Jolla, where he is currently the Inaugural Holder of the Communications Industry Chair. He is currently Director of the UCSD Center for Wireless Communications. During the 2000–2001 academic year, he was on leave with IBM Research, San Diego, CA, where he directed the development of RF integrated circuits (RFICs) for 3G applications. He has authored or coauthored over 200 papers. He holds 27 U.S. patents.

Dr. Larson was the recipient of the 1995 Hughes Electronics Sector Patent Award for his research on RF MEMS technology. He was corecipient of the 1996 Lawrence A. Hyland Patent Award of Hughes Electronics for his research on low-noise millimeter-wave high electron-mobility transistors (HEMTs), and the 1999 IBM Microelectronics Excellence Award for his research in Si/SiGe HBT technology.



Peter M. Asbeck (M'75–SM'97–F'00) received the B.S. and Ph.D. degrees from the Massachusetts Institute of Technology (MIT), Cambridge, in 1969 and 1975, respectively.

He is currently the Skyworks Chair Professor with the Department of Electrical and Computer Engineering, University of California at San Diego (UCSD), La Jolla. He was with the Sarnoff Research Center, Princeton, NJ, and the Philips Laboratory, Briarcliff Manor, NY, where he was involved in the areas of quantum electronics and GaAlAs/GaAs

laser physics and applications. In 1978, he joined the Rockwell International Science Center, where he was involved in the development of high-speed devices and circuits using III–V compounds and heterojunctions. He pioneered the effort to develop HBTs based on GaAlAs/GaAs and InAlAs/InGaAs materials and has contributed widely in the areas of physics, fabrication, and applications of these devices. In 1991, he joined UCSD. He has authored or coauthored over 250 publications. His research interests are in development of high-speed HBTs and their circuit applications.

Dr. Asbeck is a Distinguished Lecturer for the IEEE Electron Devices Society and the IEEE Microwave Theory and Techniques Society (IEEE MTT-S). He was the recipient of the 2003 IEEE David Sarnoff Award for his work on HBTs.